
KATHOLIEKE UNIVERSITEIT
LEUVEN
Proceedings of the SECOND INTERNATIONAL
SLAG VALORISATION SYMPOSIUM
THE TRANSITION TO SUSTAINABLE MATERIALS MANAGEMENT
18-20 April 2011
Leuven, Belgium
Editors: Peter Tom Jones, Yiannis Pontikes, Jan Elsen, Özlem Cizer, Luc Boehme,
Tom Van Gerven, Daneel Geysen, Muxing Guo, Bart Blanpain
Organisers:
centre
for High Temperature Processes and Sustainable Materials Management
SMART-PRO²

Additions of industrial residues for hot stage engineering of stainless steel slags

Yiannis PONTIKES[1,2], Lubica KRISKOVA[1,2], Xuan WANG[1], Daneel GEYSEN[1,2], Sander ARNOUT[3], Els NAGELS[3], Özlem CIZER[4], Tom VAN GERVEN[5], Jan ELSEN[6], Muxing GUO[1,2], Peter Tom JONES[1,2], Bart BLANPAIN[1,2]

[1] Department of Metallurgy and Materials Engineering, Katholieke Universiteit Leuven, Kasteelpark Arenberg 44 bus 2450, B-3001 Heverlee (Leuven), Belgium
[2] Centre for High Temperature Processes and Sustainable Materials Management, Department of Metallurgy and Materials Engineering, Katholieke Universiteit Leuven, Kasteelpark Arenberg 44 bus 2450, B-3001 Heverlee (Leuven), Belgium
[3] InsPyro NV, Kapeldreef 60, 3001, Leuven, Belgium
[4] Department of Civil Engineering, Katholieke Universiteit Leuven, Kasteelpark Arenberg 40, B-3001 Heverlee, Belgium
[5] Departement of Chemical Engineering, W. de Croylaan 46 Bus 2423, B-3001 Heverlee (Leuven), Belgium
[6] Department of Earth and Environmental Sciences, Katholieke Universiteit Leuven, Celestijnenlaan 200E, B-3001 Heverlee (Leuven), Belgium

yiannis.pontikes@mtm.kuleuven.be, lubica.kahalova@mtm.kuleuven.be, xuan.wang@cit.kuleuven.be, daneel.geysen@mtm.kuleuven.be, sander.arnout@inspyro.be, els.nagels@inspyro.be, ozlem.cizer@bwk.kuleuven.be, thomas.vangerven@cit.kuleuven.be, jan.elsen@ees.kuleuven.be, muxing.guo@mtm.kuleuven.be, peter.jones@mtm.kuleuven.be, bart.blanpain@mtm.kuleuven.be

Abstract

The disintegration of stainless steel slags, due to the beta to gamma dicalcium silicate transformation, hinders the valorisation and increases the landfilling cost considerably. In this work, two industrial wastes, namely boron residues from the dressing of boron minerals and fly ash from lignite's combustion, have been used as additives in order to produce physically stable stainless steel slags. Results indicate that 1 wt% of boron residue is sufficient, however, 22 wt% of fly ash is required for a synthetic slag of basicity (CaO/SiO_2) = 2. The practical implications in terms of valorisation of the produced slags are also discussed.

Introduction

Large volumes of slags are produced annually, leading to important economical and ecological issues regarding their afterlife. To maximise the recycling potential, slag processing has become an integral part of the valorisation chain.[1] Stainless steel slags

are currently used for a number of applications and some alternative routes have been suggested in literature:[2] aggregates, additives or raw materials for cement making, carbon sink, as well as fertilisers and additives for soil treatment are only a few of the potentialities. Nonetheless, disintegration of stainless steel slags hinders the valorisation and increases the landfilling cost considerably.

It is well established that this kind of disintegration is driven by the presence of dicalcium silicate ($2CaO{\cdot}SiO_2$ or C_2S) in the slag.[3] This mineral undergoes several phase transformations from one polymorph to another when the slag is cooled. As the athermal, martensitic-like transformation of the monoclinic β-polymorph to the orthorhombic γ-polymorph[4] is accompanied by a volume expansion of about 12%, high internal stresses finally cause the disintegration of the slag. The potential routes to avoid the formation of γ-C_2S are: a) chemical stabilisation by additions, b) change in slag chemistry and c) fast cooling.

In metallurgy, the option of inhibiting the *β* to *γ* transformation of C_2S was first elaborated in 1986 by Seki and co-workers,[5] who developed a borate based stabiliser for stainless steel decarburisation slag. Because of its effectiveness and simplicity, borate stabilisation of air-cooled slags is widely implemented in industrial practice. Typical minerals used are disodium tetraborate (brand name Dehybor or anhydrous Borax, $Na_2B_4O_7$) and/or colemanite ($Ca[B_3O_4(OH)_3]{\cdot}H_2O$). Results regarding the distribution of boron in the slag matrix have been reported in previous work.[6]

Borate additions are not the only possibility to avoid the expansive transformation of C_2S and the associated disintegration of the slag[7-10] The crystallographic coordination number, the ionic radius and the ionic valence of the doping ion all affect the deformation of the C_2S crystal and, as a consequence, the stabilisation. In practice, different oxides have been reported to stabilise the different polymorphs of dicalcium silicate. The α and α′ polymorphs have been reported to be stabilised by oxides such as MgO, Al_2O_3, Fe_2O_3, BaO, K_2O, P_2O_5 and Cr_2O_3. The β polymorph can be stabilised by the addition of Na_2O, K_2O, BaO, MnO_2, Cr_2O_3 or their combinations.[7] This is exemplified in cement production: the C_2S, referred to as belite, constitutes the second highest in content ingredient in ordinary Portland cement (OPC) clinker that, nonetheless, does not disintegrate during cooling. This is attributed to the fact that belite in OPC is a solid solution with an average formula (normalised to 4O): $Ca_{1.97}Mg_{0.02}Na_{0.01}K_{0.03}Fe_{0.02}Al_{0.07}Si_{0.91}P_{0.01}O_{4.00}$.[11] Typically, Al_2O_3 and Fe_2O_3 are the main impurity oxides, the total content being in the range 4-6 wt%. In principle, the above rationale could be extended to slag chemistry and stabilise C_2S by forming a solid solution with other oxides.

This work presents two cases where industrial residues were used to stabilize C_2S containing stainless steel slag. The underlying principle is that the use of a waste renders the industrial implementation more likely due to the low associated cost. Indeed, the notion of waste synergy has been fundamental in the establishment of industrial symbiosis parks and clearly contributes to sustainable development.

Experimental

Materials

Boron waste and fly ash were used in order to stabilise the synthetic slag. The boron waste originates from Turkey. Turkey possesses the largest boron deposits with a worldwide share of 72% (851 Mtonnes) in terms of B_2O_3 content. The principal borate minerals are tincalconite ($Na_2(B_4O_7)\cdot 5H_2O$), ulexite ($NaCa[B_5O_6(OH)_6]\cdot 5H_2O$) and colemanite ($Ca[B_3O_4(OH)_3]\cdot H_2O$) which are refined into pure chemical compounds.[12] During this process, approximately 400000 tonnes/year of different types of solid boron-containing wastes (BW) are produced and disposed of in tailing heaps next to the boron plant.[13] This raises substantial environmental concerns in fear of boron leaching and subsequent soil and groundwater pollution. In particular, the dissolved boron compounds form several complexes with the heavy metals (Pb, Cu, Co, Ni, Cd *etc.*), which are more toxic and soluble than their metals.[14] The B_2O_3 content in these wastes usually varies from 11 to 20 wt%, which depends on the initial minerals and the processing conditions. More information regarding the wastes can be retrieved elsewhere.[15] Already in the literature, a similar attempt was performed by Branca *et al.* using boron containing glazing powders[16] with promising results. The fly ash used in this work originates from the Megalopolis plant, Public Power Corporation, Greece. It is produced during lignite combustion and is rich in $A1_2O_3$ and Fe_2O_3, besides CaO and SiO_2. The total annual ash production in Greece is estimated between 10 and 11 Mt, of which 2.4 Mt are produced in the Megalopolis plant. The cement companies utilise typically < 15% of the produced quantity, thus a substantial amount is accumulated every year. Fly ash seems to be a good candidate as it contains most of the oxides needed for C_2S stabilisation. The reference synthetic slag was prepared from analytical grade oxides, with a chemistry close to industrial practice.

Methods

Boron waste and fly ash were preheated at 700°C. Reference slag and boron waste or fly ash, in different concentrations, were mixed in batches of 50 g and homogenised for 12 h in a rotary mixer. The final mixture was introduced in a Pt-Rh crucible and was heated in a resistance furnace (AGNI-ELT 160-02 Springtype). The firing profile

involved heating and cooling rate of 10°C/min, up to 1640°C, and a 1 hour isothermal step at 1640°C.

The thermodynamic calculations were performed by FactSage 6.2. Compound database FACT 53 and coupled compound & solution database FToxid were used together. Four solution datasets of FToxid were selected: FToxide-SLAGH, FToxide-bC2S (alpha'), FToxide-aC2S (alpha), FTOxid-Mel (melilite) and FTOxid-MeO (CaO and MgO). FACT 53 was suppressed by FToxid to exclude duplications in the data set. The stability of cuspidine was adjusted with 20 kJ for it to be stable with respect to solid oxides and CaF_2. Ti, Sr, K, Na, and S were not considered in the calculations. The chemical composition was determined using X-Ray Fluorescence spectrometry (XRF, Philips PW 2400). The particle size distribution was determined with a laser scattering technique (MasterSizer Micro Plus, Malvern). The mineralogy of the samples was determined with X-Ray Powder Diffraction analysis (XRPD, D500 Siemens). Diffraction patterns were measured in a 2θ range of 10-70° using CuKα radiation of 40 kV and 40 mA, with a 0.01° step size and step time of 3 s. Qualitative analysis was performed with the "X'pert HighScore Plus" PANalytical software. Quantitative results were obtained by adding 10 wt% of analytical grade crystalline ZnO and by refining the diffraction patterns adopting the Rietveld method.[17,18] This computer code is implemented in the "Topas® Academic" software.[19] The approach is based on a least squares refinement carried out until the best fit is obtained between the observed powder diffraction pattern and the calculated pattern. The calculated pattern is based on the simultaneously refined models for the crystal structure(s), the diffraction optics effects, the instrumental factors and other specimen characteristics (*e.g.* strain, crystallite size). Microstructural characterisation of the slag was performed using scanning electron microscopy (SEM XL30, Philips). Polished, carbon-coated samples were used, with or without Nital etching. Energy Dispersive Spectrometry (EDS) was employed for microchemical analysis. Image analysis was performed based on the image stacking technique and greyscale separation for the specific minerals.[20]

Results and discussion

The chemical composition of the reference slag, boron waste and fly ash (after heating) is presented in Table 1. In terms of mineralogy, the major crystalline phases of boron waste are tincalconite $Na_2B_4O_7{\cdot}5H_2O$ and dolomite $CaMg(CO_3)_2$. Sanidine $KAlSi_3O_8$, calcite $CaCO_3$, Chlorite $(Mg, Fe^{2+})_{10}Al_2[(Si_6Al_2)O_{20}](OH)_{16}$, montmorillonite $(0.5Ca,Na)_{0.7}(Al,Mg,Fe)_4[(Si,Al)_8O_{20}](OH)_4{\cdot}nH_2O$ and most probably searlesite $NaBSi_2O_5(OH)_2$, are also present as minor phases. Fly ash is composed of quartz (SiO_2), anorthite ($CaAl_2Si_2O_8$), magnetite (Fe_3O_4), anhydrite ($CaSO_4$) and gehlenite ($Ca_2Al_2SiO_7$).

Table 1: Chemical composition of boron waste and fly ash, in wt%. n.d. : not determined; - : not present

	SiO_2	Al_2O_3	Fe_2O_3	CaO	MgO	SrO	K_2O	Na_2O	B_2O_3	SO_3	TiO_2	CaF_2	other
Synthetic slag	28.4	1.3	-	56.7	6.5	-	-	-	-	-	1.1	6.0	-
Boron waste	21.9	3.6	1.0	18.2	14.1	2.8	2.4	9.2	25.8	n.d.	n.d.	n.d.	1.0
Fly ash	50.2	19.5	9.2	11.7	2.5	n.d.	2.2	0.3	n.d.	3.0	0.8	n.d.	0.6

Reference slag

After cooling at room temperature, the slag was totally disintegrated into a light-yellow, fine powder. The d_{10}, d_{50} and d_{90} are 7.7 µm, 37.8 µm and 150.4 µm, respectively. SEM analysis reveals that the particles have an extensive network of cracks, as a result of the accumulation of high internal stresses during cooling. The results from the thermodynamic calculations at 20°C and 1650°C and from the Rietveld analysis on the solidified slag are reported in Table 2. At 1650°C, the thermodynamic calculations predict that the liquid slag amounts to 71 wt% approximately, with α-C_2S and a small amount of MgO and CaO still existing in the system. On the condition of equilibrium cooling, Fig. 1, α-C_2S transforms to α'_H-C_2S at 1425°C, approximately. The liquid phase totally disappears at around 1200°C.

Table 2: Crystalline phases predicted by FactSage thermodynamic calculations and determined by XRD and Rietveld quantitative phase analysis, for the reference slag

Phase	Thermodynamic calculation (wt%)			XRD analysis 20°C (wt%)
	Equilibrium cooling, 20°C	Scheil-Gulliver cooling, 20°C	1650°C	
CaO	6.3	9.1	1.0	
α-C_2S		49.1	25.1	
α'-C_2S		14.5		
β-C_2S				0.8
γ-C_2S	55.4			42.7
MgO	7.0	3.1	3.3	7.4
$Ca_3Mg(SiO_4)_2$				20.6
CaF_2		1.9		0.5
$Ca_4Si_2O_7F_2$	28.6	19.6		28.1
$Ca_3MgAl_4O_{10}$	2.6	2.6		
Liquid slag			70.6	

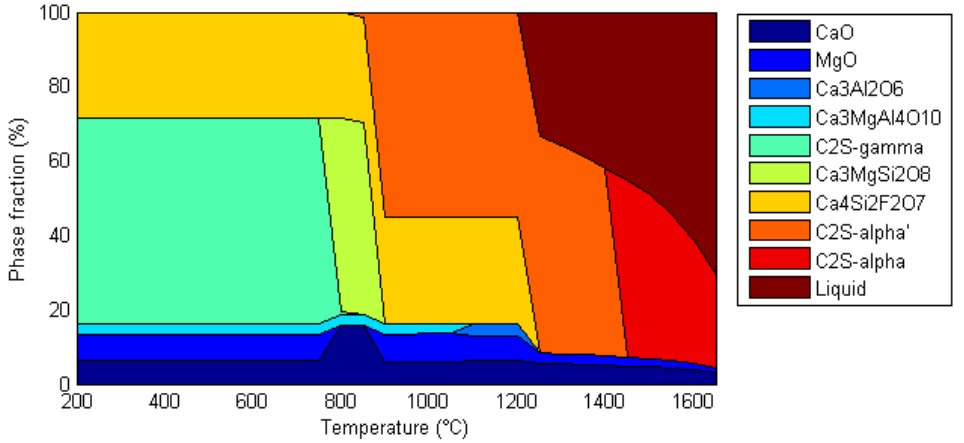

Figure 1: FactSage thermodynamic calculations based on equilibrium cooling for the reference slag

For the temperature interval 1200 to 1100°C, $Ca_3Al_2O_6$ precipitates, whereas from 850 to 800°C, $Ca_3MgSi_2O_8$ (merwinite) appears. The phase $Ca_4Si_2F_2O_7$ (cuspidine) precipitates at 1200°C and at 1050°C, $Ca_3MgAl_4O_{10}$ forms. Eventually, at room temperature the major phases predicted are γ-C_2S and cuspidine, with a small amount of CaO, MgO and $Ca_3MgAl_4O_{10}$. On the condition of Scheil-Gulliver cooling (*i.e.* no diffusion in the solids, rapid diffusion in the liquids, and equilibrium at solid/liquid interfaces), Fig. 2, the amount of α'_H-C_2S, CaO and MgO increase as the liquid slag progressively cools. At 1000°C, the slag solidifies and fluorite, cuspidine and $Ca_3MgAl_4O_{10}$ form. This fact is indicative of the F enrichment in the slag phase. At room temperature, the major phases are α-C_2S, α'_H-C_2S and cuspidine, with smaller amounts of CaO, MgO, $Ca_3MgAl_4O_{10}$ and fluorite. Due to the Scheil-Gulliver assumption, the results do not predict the formation of γ-C_2S, however, the total amount of C_2S is comparable in both equilibrium and Sheil-Gulliver cooling. Results from Rietveld analysis reveal that the main phase is γ-C_2S, with substantial amounts of merwinite, cuspidine, as well as periclase, and traces of fluorite and β-C_2S.

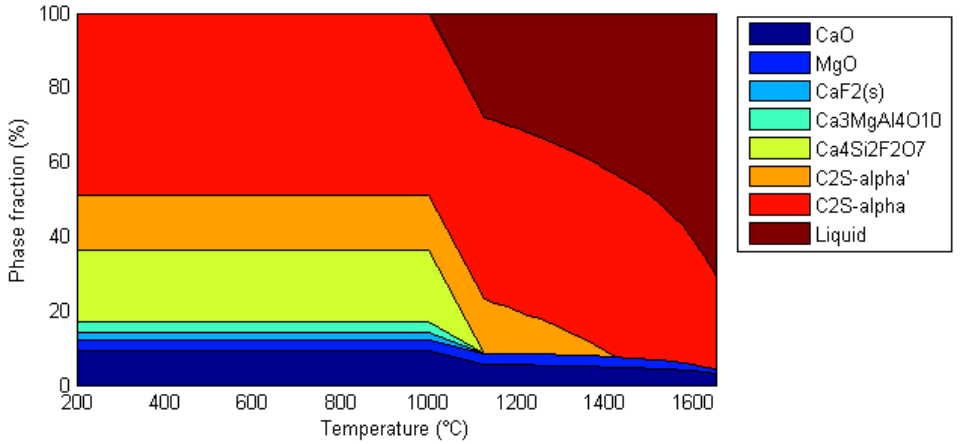

Figure 2: FactSage thermodynamic calculations based on Scheil-Gulliver cooling for the reference slag.

Stabilisation with boron

In order to stabilise the synthetic slag, boron waste was added at 0.6 wt%, 0.8 wt% and 1.0 wt%. The first two trials were partially successful as only a part of the slag was stabilised; the last trial at 1.0 wt% resulted to a dense, light-brown slag. This amount corresponds to 0.26 wt% of B_2O_3 that is close to reported values for a comparable slag composition.[5] The results from the Rietveld analysis on the solidified slag, Table 3, reveal that the main phase is β-C_2S, with α′-C_2S, cuspidine, fluorite, periclase and merwinite constituting the rest of the matrix. Comparison of these results with the ones for the reference slag, demonstrates that the difference is not limited to C_2S. Indeed, the addition of only 1 wt% of boron waste is resulting to a substantially different mineralogical assemblage at room temperature. Besides the stabilisation of β-C_2S, the main changes relate to the formation of merwinite and cuspidine. A plausible hypothesis is that the different mineralogical forms of C_2S react differently with the matrix during solidification. FactSage calculations have not been performed for this system. The effect of 1 wt% is too small to be reflected in the calculation and, moreover, B is not fully modelled yet in the software.

Table 3: Crystalline phases determined by XRD and Rietveld quantitative phase analysis, for the 1 wt% boron waste-stabilised slag

Mineral	XRD analysis, 20°C (wt %)
α′-C_2S	8.9
β-C_2S	66.2
MgO	9.1
$Ca_3Mg(SiO_4)_2$	3.2
CaF_2	4.0
$Ca_4Si_2O_7F_2$	8.6

The microstructure of boron stabilised slag consists predominantly of large, well developed crystals of β-C_2S, Fig. 3. Dimensions of the grains vary greatly; however, length can be higher than 2.00 μm. Most C_2S crystals present parallel striations, *i.e.* twinning, as seen in Fig. 4. Two different twinning modes of β-C_2S have been reported: (i) both {100} and {001}-type[21] and (ii) only {100}-type twinning.[22] Twinning has been associated with grain size and results reported by Nettleship *et al.* by TEM studies suggest that twins exist in the range of 0.04 μm to 0.2 μm for grain sizes in the range 1 to 5 μm.[23] This morphology is also found in cement clinkers, although not commonly.[24] They are typically found in clinkers produced at a very low temperature or cooled very slowly,[25] the latter being the case also in the present work. According to Insley's classification of belite in cement clinkers,[26] this is type II belite.

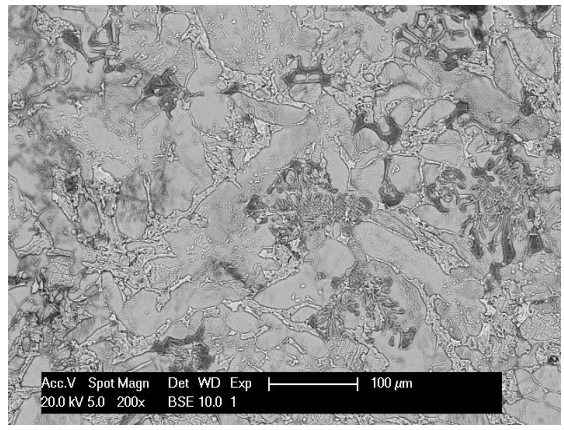

Figure 3: Backscattered electron image on the 1 wt% boron waste-stabilised slag after chemical etching.

At the grain boundaries a number of phases are located, such as periclase, bredigite, titanates, cuspidine, fluorite and alumina. Periclase exists as an inclusion also in belite. The above are visualised in Fig. 5. On the left, the backscattered electron image (BEI) on boron-waste stabilised slag is presented, whereas on the right, the distribution of phases is shown. The latter image has been constructed based on the elemental maps for O, Ca, Si, Mg, F, Al and Ti. It appears that β-C_2S is the major phase. Periclase grains are also evident. Bredigite has formed between β-C_2S and periclase, whereas Ti is associated also with Al and Ca. Cuspidine exists in the grain boundaries of β-C_2S and most probably Al dissolves also in the lattice forming a solid solution. Small grains of Al_2O_3 and Fluorite are also present.

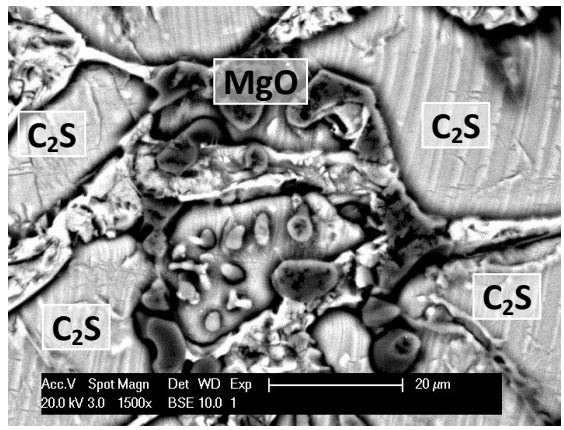

Figure 4: Backscattered electron image on the 1 wt% boron waste-stabilised slag after chemical etching.

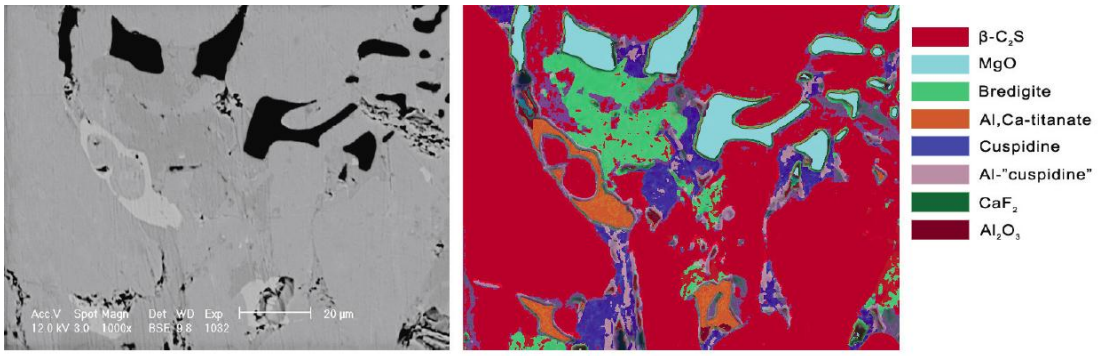

Figure 5: Backscattered electron image (left) and phase distribution based on image stacking from elemental maps (right) of 1 wt% boron waste-stabilised slag

Stabilisation with fly ash

Three additions of fly ash were studied, 14, 18 and 22 wt%, the latter being successful in terms of stabilisation. It is obvious that eventually fly ash stabilises the system not through impurities in the C_2S crystal lattice but rather by avoiding its formation. Indeed, as stated elsewhere,[27] γ-C_2S formation is prevented for a CaO/SiO_2 (weight ratio) value below 1.4. In the present case, the CaO/SiO_2 for the stabilised sample is 1.42.

Thermodynamic calculations predict that at 1500°C no solid phase remains in the system. On the condition of equilibrium cooling, Fig. 6, α'_H-C_2S and merwinite are the first phases to precipitate at 1350°C, approximately. Almost at the same temperature, 1300°C, $melilite_{ss}$ (the subscript denoting solid solution, formula is $Ca_2Al_{1.7}Fe_{0.25}Mg_{0.03}Si_{1.04}O_7$) forms, whereas cuspidine precipitates for T < 1200°C. The system is totally solidified at 1100°C. Between 1050°C and 1000°C, the amount of melilites and α'_H-C_2S decrease and rankinite ($Ca_3Si_2O_7$), gehlenite (Al-melilite), $CaFe_2O_4$ and additional merwinite form. At 600°C, cuspidine reacts towards rankinite and fluorite. Finally for T < 300°C, merwinite, gehlenite, $CaFe_2O_4$ react and produce $CaMg_2Al_{16}O_{27}$, more γ-C_2S and rankinite, as well as $Ca_3Fe_2Si_3O_{12}$. On the condition of Scheil-Gulliver cooling, merwinite, $melilite_{ss}$, α'_H-C_2S and cuspidine are the main phases predicted at room temperature. Rietveld analysis reveals that melilites, *i.e.* gehlenite and åkermanite, constitute the main phase, 34.3 wt%. Bredigite, merwinite and cuspidine account for the rest. Other phases, such as β-C_2S, seem also probable. However, the analysis is not conclusive due to peak overlapping. Nonetheless, SEM analysis does verify the existence of C_2S. Comparing the thermodynamic results with Rietveld analysis, Scheil-Gulliver cooling was able to predict the formation of melilites and cuspidine. However, the level of C_2S was probably overestimated in both cases.

Table 4: Crystalline phases predicted by FactSage thermodynamic calculations and determined by XRD and Rietveld quantitative phase analysis, for the 22 wt% fly ash-stabilised slag.

Mineral	Thermodynamic calculation (wt%)			XRD analysis, 20°C (wt%)
	Equilibrium cooling, 20°C	Scheil-Gulliver cooling, 20°C	1500°C	
$Ca_2Al_2SiO_7$		24.9 *		30.6
$Ca_2MgSi_2O_7$				3.7
$Ca_7MgSi_4O_{16}$				22.8
$Ca_3MgSi_2O_8$	44.3	37.1		24.9
$Ca_4Si_2O_7F_2$		15.2		18.0
$Ca_3Si_2O_7$	17.5			
$Ca_3Fe_2Si_3O_{12}$	5.5			
$CaMg_2Al_{16}O_{27}$	5.6			
α'-C_2S		20.5		
γ-C_2S	22.0			
CaF_2	5.0	1.8		
Liquid slag			100	

* : the calculated melilite is a solid solution with formula $a_2Al_{1.7}Fe_{0.25}Mg_{0.03}Si_{1.04}O_7$

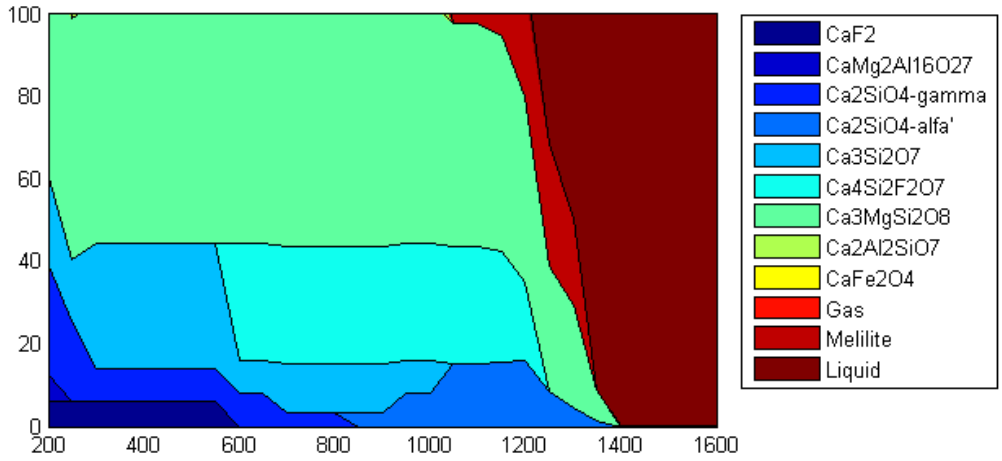

Figure 6: FactSage thermodynamic calculations based on equilibrium cooling for the 22 wt% fly ash-stabilised slag

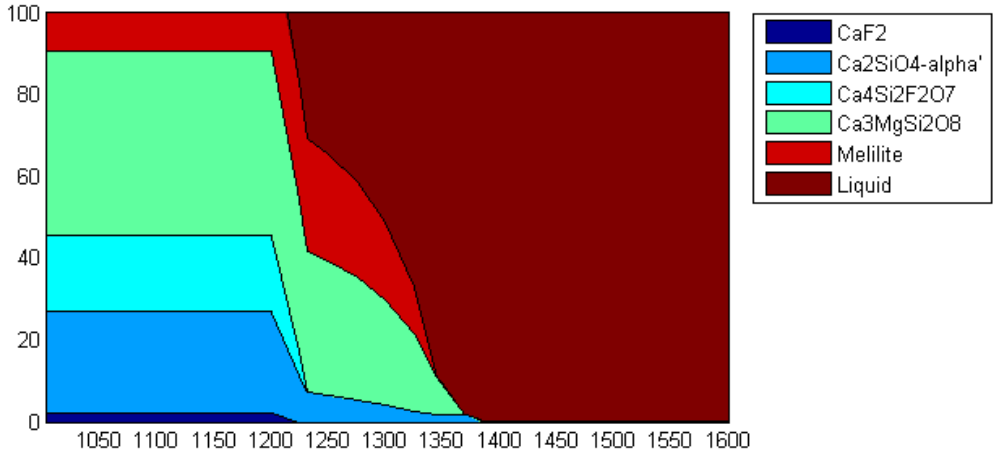

Figure 7: FactSage thermodynamic calculations based on Scheil-Gulliver cooling for the 22 wt% fly ash-stabilised slag

SEM results are presented in Fig. 8. The BEI of the microstructure appears left and the phase distribution appears right. At the upper left section, cuspidine is identified. Gehlenite surrounds cuspidine formation and gradually (moving from gehlenite lower) the composition changes to akermanite. This is probably the result of Mg diffusion from bredigite. Due to very close atomic numbers of Al and Mg, this subtle variation is not apparent in terms of grey intensity in the BEI. Merwinite is typically adjacent to bredigite and is distinct also in terms of morphology. Dicalcium silicate is found in a number of locations and typically appears as a porous formation. It seems most probable γ-C_2S, however, it is not certain if it was originally gamma or if this is the result of sample preparation. Titanium appears in distinct grains and is associated with Fe, probably in the form of Fe-titanate.

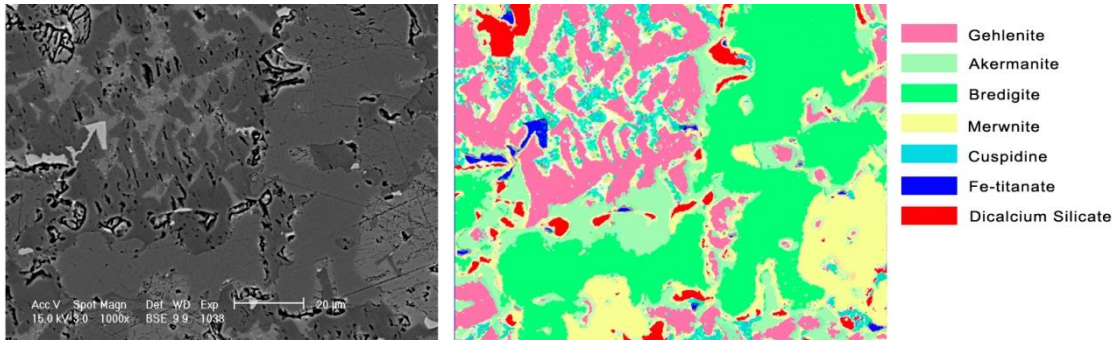

Figure 8: Backscattered electrons' image (left) and phase distribution based on image stacking from elemental maps (right) of the 22 wt% fly ash stabilised stainless steel slag

Practical implications

In the case of boron waste stabilised slag, the results are promising as the final product is both physically stable and hydrates towards C-S-H after milling (results not reported herein). Thus, in principle, this slag exhibits the potential to be used in applications as aggregate or as a hydraulic binder. Obviously the use as a hydraulic binder increases the value of the slag in the market, however, (stainless) steel slags can not constitute part of the blended cements in Europe from a regulatory point of view (EN 197-1). Therefore, other applications such as cement blocks, screed material, or binder for pelletising applications appear more realistic.

In other countries, different regulations are in place. For instance, according to the Chinese YB/T022-92 standard, a steel slag cement is produced with 65% clinker and 35% ground BOF slag whereas results were published recently on the use of AOD slag in blended cements in China.[28] In its endeavour to strengthen sustainability through regulatory policy, it is possible that future regulations in Europe may adapt to new criteria. As mentioned elsewhere,[29] the new prEN 13282 (draft) includes BOF slag as possible main component of Hydraulic Road Binders, up to 40 wt%. Thus, future regulations in Europe may also integrate stainless steel slags, provided they hydrate at a considerable extent and demonstrate an environmentally sound behaviour.

In the case of fly ash addition, stabilisation did not result as a consequence of impurities in the crystal lattice of C_2S, but merely by driving the system out of the C_2S stability field. This has been suggested already in 1942, where compositional limits were defined for disintegrating slags,[30] based on the stability field of C_2S in the CaO-MgO-SiO_2-Al_2O_3 system, with an adjustment for the sulphur content (S) in the slag:

$$CaO + 0.8\ MgO \leq 1.20\ SiO_2 + 0.39\ Al_2O_3 + 1.75\ S$$
$$CaO \leq 0.93\ SiO_2 + 0.55\ Al_2O_3 + 1.75\ S$$

Thus, fly ash addition in the present work acted as SiO_2, Al_2O_3 and S source. In the same direction, Sakamoto,[31] stabilised a stainless steel decarburisation slag with 12 wt% of waste glass, containing 70-75 wt% SiO_2, Eriksson and B. Björkman[32] stabilised low-basicity stainless steel slag by adding MgO, whereas Kitamura *et al*.[33] suggested the addition of cold or preheated non-ferrous fayalite slag to stainless steel slag in order to reduce the basicity. In the latter case the FeO from the non-ferrous slag is used as an additional energy source (exothermic reaction to Fe_2O_3 results in additional heat) to dissolve the SiO_2. Nonetheless, the scale up of these processes to industrial level is not straightforward as the dissolution of the additions appears to be the critical point. It is possible that an additional heat source or even slag treatment process would be required. At least for the present case, addition of 22 wt% fly ash for the production of aggregates does not seem realistic.

Conclusions

Increasing environmental awareness has created incentives for metallurgical companies to tackle various slag issues. Regarding stainless steel slags, C_2S-driven disintegration during cooling is one of the main issues, as it not only creates dust problems but also complicates the slag valorisation in construction applications. Boron waste addition proves to be an effective alternative to other boron sources currently in use. A 1 wt% addition resulted to the stabilisation of a slag with basicity (CaO/SiO_2) = 2. Addition of fly ash stabilises the system by diverting the slag chemistry outside the C_2S stability field, effectively showing that fly ash functions as a SiO_2, Al_2O_3 and S source. An addition of 22 wt% fly ash was required. The industrial feasibility of the fly ash route can be questioned. The resulting slags were physically stable and the boron stabilised one exhibits hydraulic properties (results not reported herein). Further analysis is required to demonstrate the performance and the environmental behaviour of such hydraulic binders.

Acknowledgements

Yiannis Pontikes is thankful to the Research Foundation – Flanders for the post-doctoral fellowship.

References

1. D. Durinck, F. Engström, S. Arnout, J. Heulens, P.T. Jones, B. Björkman, B. Blanpain and P. Wollants, “Hot stage processing of metallurgical slags”. *Resour. Conserv. Recy.,* **52** (10) 1121-1131, (2008).
2. D. Geysen, P.T. Jones, A. Sander, Y. Pontikes, Ö. Cizer, T. Van Gerven, M. Craps, J. Eyckmans and B. Blanpain, “'Slag valorisation', as an example of high temperature industrial ecology”. in *EPD Congress 2010. 2010 TMS Annual Meeting & Exhibition*, 2010, Washington State Convention Center. Vidal, E., Ed. pp. 877-884 (2010).
3. L. M. Juckes, “Dicalcium silicate in blast-furnace slag: a critical review of the implications for aggregate stability”. *Mineral Processing and Extractive Metallurgy: Transactions of the Institute of Mining and Metallurgy, Section C,* **111** 120-128, (2002).
4. G. H. Thomas and I. M. Stephenson, “The beta to gamma dicalcium silicate phase transformation and its significance on air-cooled slag stability”. *Silic. Ind.*, 195-200, (1978).
5. A. Seki, Y. Aso, M. Okubo, F. Sudo and K. Ishizaka, “Development of dusting prevention stabilizer for stainless steel slags”. *Kawasaki Steel Giho,* **18** (1) 20-24, (1986).
6. D. Durinck, S. Arnout, G. Mertens, E. Boydens, P. T. Jones, J. Elsen, B. Blanpain and P. Wollants, “Borate distribution in stabilized stainless-steel slag”. *J. Am. Ceram. Soc.,* **91** (2) 548-554 (2008).
7. S. N. Ghosh, P. B. Rao, A. K. Paul and K. Raina, “Review. The chemistry of dicalcium silicate mineral”. *J. Mater. Sci.,* **14** (7) 1554-1566 (1979).
8. A. Ghose, S. Chopra and J. F. Young, “Microstructural characterization of doped dicalcium silicate polymorphs”. *J. Mater. Sci.,* **18** (10) 2905-2914 (1983).
9. G. C. Lai, T. Nojiri and K. i. Nakano, “Studies of the stability of β-Ca_2SiO_4 doped by minor ions”. *Cem. Concr. Res.,* **22** (5) 743-754 (1992).

10. J. Geiseler, “Properties of iron and steel slags regarding their use”. In *6th Conference on molten slags, fluxes and salts*, (2000).
11. H. F. W. Taylor, *Cement Chemistry*. 2nd ed., (1997).
12. R. Smith, A., “Basic geology and chemistry of borate”. *Am. Ceram. Soc. Bull.,* **81** (8) (2002).
13. European Commission, *Reference Document on Best Available Techniques for Management of Tailings and Waste-Rock in Mining Activities*, 2004.
14. R. Boncukcuoglu, M. M. Kocakerim, E. Kocadagistan and M. T. Yilmaz, “Recovery of boron of the sieve reject in the production of borax”. *Resour. Conserv. Recy.,* **37** (2) 147-157 (2003).
15. T. Kavas, A. Christogerou, Y. Pontikes and G. N. Angelopoulos, “Valorisation of different types of boron-containing wastes for the production of lightweight aggregates”. *J. Hazard. Mater.,* **185** (2-3) 1381-1389 (2011).
16. T. A. Branca, V. Colla and R. Valentini, “A way to reduce environmental impact of ladle furnace slag”. *Ironmaking and Steelmaking,* **36** 597-602 (2009).
17. H. M. Rietveld, “A method for including the line profiles of neutron powder diffraction peaks in the determination of crystal structures”. *Acta Crystallogr.,* **21** A228 (1966).
18. H. M. Rietveld, “A profile refinement method for nuclear and magnetic structures”. *J. Appl. Crystallogr.,* **2** 65-71 (1969).
19. A. A. Coelho, “TOPAS-Academic; A Computer Programme for Rietveld Analysis”. http://www.topas-academic.net/, (2004).
20. J. W. Lydon, *The measurement of the modal mineralogy of rocks from SEM imagery: the use of Multispec © and ImageJ freeware*, Geological Survey of Canada, Open File 4941, 2005, p 37.
21. D. K. Smith, A. Majumdar and F. Ordway, “The crystal structure of [gamma]-dicalcium silicate”. *Acta Crystallogr.,* **18** (4) 787-795 (1965).
22. G. W. Groves, “Twinning in [beta]-dicalcium silicate”. *Cem. Concr. Res.,* **12** (5) 619-624 (1982).
23. I. Nettleship, K. G. Slavick, K. Youn Joong and W. M. Kriven, “Phase transformations in dicalcium silicate. I: Fabrication and phase stability of fine-grained β phase”. *J. Am. Ceram. Soc.,* **75** (9) 2400-2406 (1992).
24. D. H. Campbell, *Microscopical Examination and Interpretation of Portland Cement and Clinker*. 2nd ed., Portland Cement Association, Skokie, IL 60077-1083, USA, (1999).
25. Y. Ono, *Ono’s Method, Fundamental Microscopy of Portland Cement Clinker*, Chichibu Onoda Cement Corp., 1995, p 229.
26. H. Insley, “Structural Characteristics of Some Constituents of Portland Cement Clinker, Research Paper RP917”. *Journal of Research of the National Bureau of Standards,* **17** 353-361 (1936).
27. S. Akira, A. Yoshio, O. Makoto, S. Fumio and I. Kunihiko, *Development of Dusting Prevention Stabilizer for Stainless Steel Slag*, Kawasaki Steel Technical Report, 1986, pp 16-21.
28. R. Wang and R. Chen, “Beneficial use of stainless steel AOD slag as composite cement admixture and its safety analysis”. In *Waste Recovery in Ironmaking and Steelmaking Processes*, 2010, London.
29. J.-M. Delbecq, “Steel Slags as cementitious materials”. In *Seminário Internacional - Aplicação de Escória de Aciaria*, 2010, Belo Horizonte, Brazil.
30. T. W. Parker and J. F. Ryder, “ Investigations on ‘falling’ blast furnace slags”. *Journal of the Iron and Steel Institute,* **11** 21-51 (1942).
31. N. Sakamoto, “Effects of MgO based glass addition on the dusting of stainless steel slag (development of control process of stainless steel slag dusting-3)”. *Current Advance in Materials and Processes,* **14** (4) 939 (2001).
32. J. Eriksson and B. Björkman, “MgO Modification of Slag from Stainless Steelmaking”. In *7th Conference on Molten Slags, Fluxes and Salts*, 2004, Cape Town, South Africa. Pistorius, C., Ed.
33. S. Kitamura and N. Maruoka “Modification of stainless steel refining slag through missing with nonferrous smelting slag”. In *First International Slag Valorisation Symposium*, 2009, Leuven, Belgium. Jones, P.T., Geysen, D., Guo, M. and Blanpain, B., Eds.